Title

ON THE NATURE OF STRAIN HARDENING IN POLYCRYSTALLINE ALUMINUM AND ALUMINUM-MAGNESIUM ALLOYS

Authors

Mitra, Sandip K.
Dorn, John E.

Publication Date

1962-12-22

UCRL-10365 Rev.

University of California

Ernest O. Lawrence Radiation Laboratory

ON THE NATURE OF STRAIN HARDENING IN POLYCRYSTALLINE ALUMINUM AND ALUMINUM-MAGNESIUM ALLOYS

Berkeley, California

DISCLAIMER

Submitted to Transactions American Institute of Mining and Metallurgical Engineers

UCRL-10365 rev.

UNIVERSITY OF CALIFORNIA

Lawrence Radiation Laboratory
Berkeley, California

Contract No. W-7405-eng-48

ON THE NATURE OF STRAIN HARDENING IN POLYCRYSTALLINE ALUMINUM AND ALUMINUM-MAGNESIUM ALLOYS

by

Sandip K. Mitra and John E. Dorn

revised by J. E. Dorn
December 22, 1962

LIST OF FIGURE CAPTIONS

for

"ON THE NATURE OF STRAIN HARDENING IN POLYCRYSTALLINE ALUMINUM AND ALUMINUM-MAGNESIUM ALLOYS"

by

Sandip K. Mitra and John E. Dorn

ON THE NATURE OF STRAIN HARDENING IN POLYCRYSTALLINE ALUMINUM AND ALUMINUM-MAGNESIUM ALLOYS

Sandip K. Mitra and John E. Dorn
revised by J. E. Dorn
December 22, 1962

Lawrence Radiation Laboratory
University of California
Berkeley, California

ABSTRACT

The Basinki-modified Seeger equation for deformation of metals by means of thermally activated intersection of dislocations was used to ascertain the various factors responsible for the strain hardening of polycrystalline Al and a series of alpha solid solutions of Mg in Al. The analyses were based principally on the rate of change of strain rate with stress and the Cottrell-Stokes ratio. From measurements of these quantities on a series of strain-hardened states, the force displacement diagram for intersection, the density of dislocations in the entanglements, and the contributions of the athermal local stress and long-range stress interactions were deduced.

Polycrystalline Al was observed to have the same force-displacement diagram for intersection as single Al crystals, and the corresponding diagram for the Mg alloys differed in a manner that suggested that small amounts of Mg may decrease slightly the stacking fault energy of Al. Although polycrystalline Al had about the same initial density of dislocations as the single crystals, the density of dislocations increased much more rapidly with strain in the polycrystals. This factor and the higher back

stresses generated in the polycrystalline Al were the major factors responsible for the higher strength of the polycrystalline Al.

As the Mg content of the alloys was increased, the initial density of the dislocations also increased. Most of the alloy strengthening arose from this factor; alloying effects due to short-range order strengthening, Suzuki locking, Cottrell pinning, etc. were estimated to be quite small. The greater rate of strain hardening in the alloys was deduced to be due primarily to the greater increase in the density of the dislocations with strain as the Mg content was increased.

ON THE NATURE OF STRAIN HARDENING IN POLYCRYSTALLINE ALUMINUM AND ALUMINUM-MAGNESIUM ALLOYS

Sandip K. Mitra* and John E. Dorn**

Lawrence Radiation Laboratory
University of California
Berkeley, California

December 22, 1962

I. INTRODUCTION

It is the purpose of the present investigation to shed additional light on the average plastic behavior of a grain in a polycrystalline aggregate, by analyses, based on dislocation theory, of appropriate experimental test results. These deductions when compared with those from single-crystal data will then serve to illustrate the major items of difference between the plastic behavior of single crystals and the average behavior of a grain in a polycrystalline aggregate. Effects of alpha solid solution alloying on the plastic behavior of Al were also investigated in terms of the dislocation intersection model.

Previous investigations on the plastic behavior of single crystals of face-centered cubic metals by Mitra, Osborne, and Dorn[1] and more recently by Mitra and Dorn[2] have shown, as previously emphasized by Seeger,[3] that the low-temperature thermally activated dislocation process is that of mutual intersection of dislocations. Consequently, the Seeger equation

$$\dot{\gamma} = NAb\nu e^{-U/kT} \qquad (1)$$

*Postdoctoral research metallurgist, Lawrence Radiaiton Laboratory

**Professor of Materials Science, Department of Mineral Technology, University of California, Berkeley

applies, where $\dot{\gamma}$ is the shear strain rate, N is the number of points per unit volume where intersection is imminent, A is the average area swept out by the glide dislocation per mutual intersection, b the Burgers vector, ν a frequency about equal to the Debye frequency, U the activation energy for intersection, k the Boltzmann constant, and T the absolute temperature. Although the energy for intersection depends on the intimate geometric details of the process, as revealed by Schoeck and Seeger,[4] we make the customary assumption here that the variables in Eq. 1 represent suitable smeared average values. Whereas Seeger assumed that the activation energy, U , decreases linearly with the applied stress, Basinski[5] has shown that, in fcc metals, owing to the constriction of the partials and the bowing of the intersected dislocation, a more appropriate relationship is given by

$$u = \int_{F}^{F_m} x\, dF \tag{2}$$

The F_o - x diagram for intersection, as shown for single crystals of pure Al,[1] in Fig. 1, represents the average force-displacement diagram at the absolute zero. At temperatures above the absolute zero, however, the force for any displacement varies linearly with the shear modulus of elasticity, G , and is given by

$$F = F_o\, G/G_o \tag{3}$$

The values of G/G_o for Al used throughout this paper for both pure Al and the Al-Mg alloys were calculated for the slip direction on the slip plane from the data reported by Sutton.[6] The force F is given by

$$F = (\tau - \tau^*) L b = (\tau - \tau_o^* G/G_o) L b \tag{4}$$

where τ_o^* is the total back-stress field, referred to the absolute zero, that cannot be overcome by a thermal fluctuation. Whereas Hirsch[7] and Basinski[11] have suggested that τ_o^* arises only from the local stress fields at the point of intersection, Mitra and Dorn[2] have shown that

$$\tau^* = \tau_i^* + \tau_\ell^* \tag{5}$$

for pure metals, where

$$\tau_i^* = \frac{\alpha G b}{L} \tag{6}$$

gives the local stress effect due to interactions of the glide and forest dislocations, and τ_ℓ^* arises from long-range stress fields and other athermal restraints on dislocation motion. Mitra and Dorn[2] have found, experimentally, that the average value of $\alpha = 0.035$ applies to Al. This latter value will be assumed throughout this paper for polycrystalline Al and the Al-Mg alloys.

A satisfactory description of the origin of the long-range back stresses is not yet known. Whereas Seeger[3] and Friedel[8] originally ascribed these stresses to piled-up dislocation arrays, such arrays are not usually seen in electron microscopic investigations, particularly in high-stacking-fault metals such as Al. We might suggest, however, that they can arise from concentrations of dislocations of the same sign in certain regions, and they may also be associated with effects due to the commonly observed dislocation entanglements in cold-worked Al in two possible ways. One is merely a result of the concentration of dislocations of the same sign in a given region; and the second is due to the fact that entanglements may represent a lower energy state; consequently, forcing a dislocation segment from an entanglement may require that some

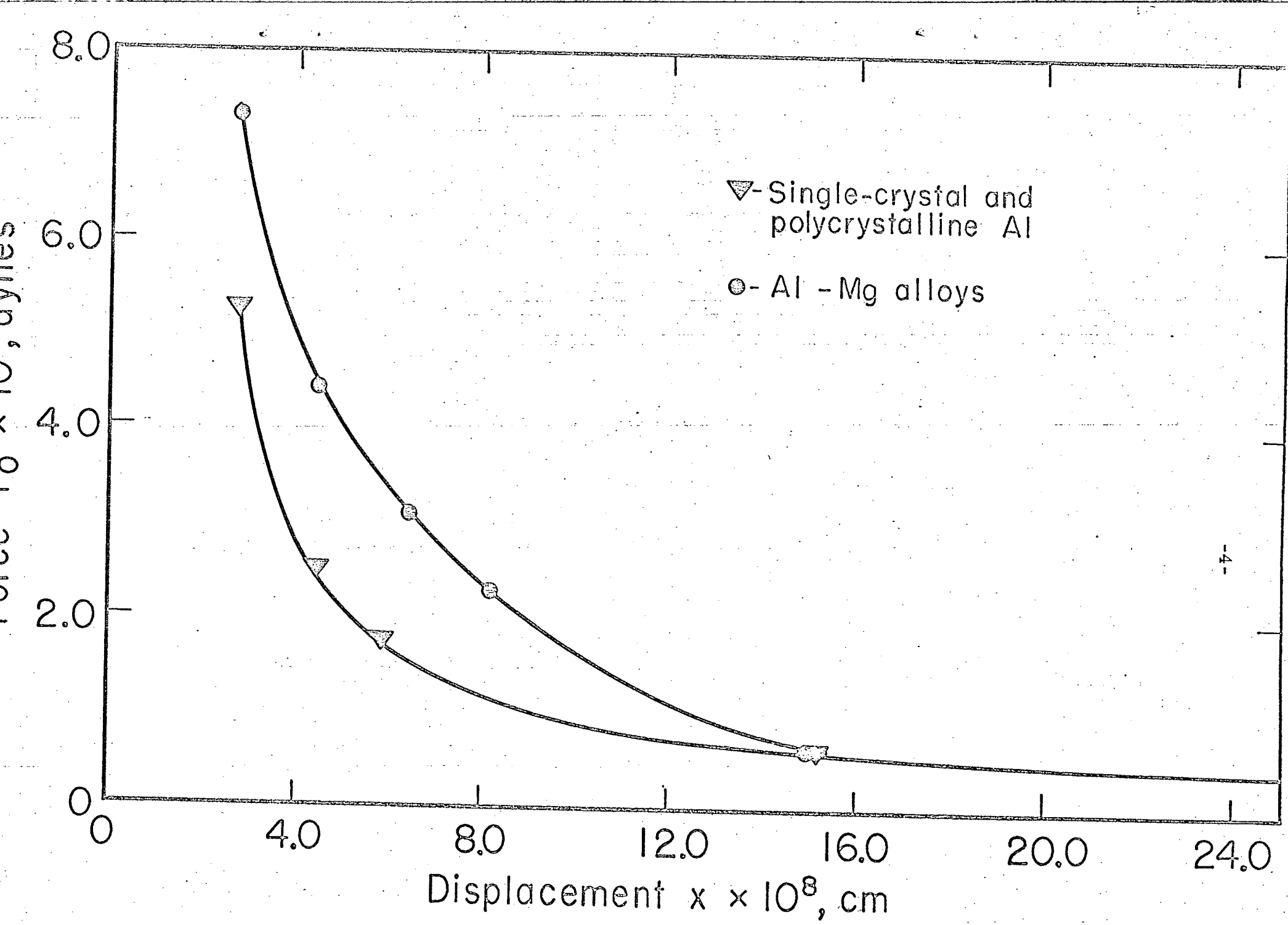

Fig. 1 Force-displacement curves for dislocation intersection in pure Al and Al-Mg alloys.

work be done against the attractive stress fields of the residual dislocations in the entanglement. Other athermal restraints on the motion of dislocations such as might result from jog formation, trails and debris also contribute to the value of τ_ℓ^* . In Al alloys we expect another contribution, τ_S^* , to the back-stress field arising from the effects of short-range order Suzuki locking, etc. Therefore, for alloys, one has

$$\tau^* = \tau_\ell^* + \tau_S^* + \frac{\alpha G b}{L} \qquad (7)$$

The objective of this investigation is to deduce the F_o - x curve as well as the dependence of $1/L$ and τ^* on the plastic strain for polycrystalline Al and Al-Mg solid solution alloys. The F_o - x curve for polycrystalline high-purity Al will be shown to be identical with that obtained from single-crystal data. This agreement is required when the theory is reliable, the same slip systems predominate, and the deformation is controlled by the same thermally activated mechanism in single crystals and polycrystals. The F_o - x curve for the alloys, however, will be shown to differ slightly from that for high-purity Al, as might be expected if small amounts of alloying with Mg decreases the stacking-fault energy. Our major interest, however, will be the trends of τ^* and $1/L$ with the strain, since these factors describe the work-hardening characteristics. We will show that the strain hardening of polycrystals differs from that of single crystals, and that solid-solution alloying also affects the strain-hardening trends.

II. EXPERIMENTAL PROCEDUCRES AND RESULTS

Tensile specimens with their longitudinal axes in the rolling direction were machined from 0.1-in. thick sheets of the Al alloys, the chemical compositions of which are given in Table I. The reduced sections were 3 in. long and 0.250 in. wide. In order to obtain the same average grain diameter of 0.3 mm the alloys were given the heat treatments shown also in Table I. Each specimen was etched before testing to reduce the possible effect of oxide coatings on the test results.

Table I. Chemical composition and heat treatment of the alloys

	Chemical composition by weight %						Heat treatment	
Alloys	Mg	Cu	Fe	Si	Others	Al	Temp. (°F)	Time (min)
Pure Al	0.000	0.002	0.000	0.004	0.000	bal.	650	30
Alloy (i)	0.970	0.001	0.002	0.003	0.000	bal.	850	30
Alloy (ii)	1.790	0.001	0.002	0.004	0.000	bal.	850	45
Alloy (iii)	2.820	0.001	0.002	0.004	0.000	bal.	850	60

Tension tests were made with an Instron testing machine operated at a strain rate of $\dot{\varepsilon} = 1 \times 10^{-4}$ per sec. Stresses were determined to within $\pm 2 \times 10^{6}$ dyn/cm^2, and tensile strains were measured to within ± 0.0001. To maintain constant temperatures, the entire specimen was immersed in one of a series of constant boiling temperature baths.[1] The diagrams of true stress vs true strain that were obtained at 90°K are shown in Fig. 2.

In order to obtain data for calculating the activation volume, the values of β, defined by

$$\beta = \left(\frac{\partial \ln \dot{\varepsilon}}{\partial \tau}\right)_T \simeq \left(\frac{\ln \dot{\varepsilon}_2/\dot{\varepsilon}_1}{\tau_2 - \tau_1}\right)_T \simeq \left(\frac{2 \ln \dot{\varepsilon}_2/\dot{\varepsilon}_1}{\sigma_2 - \sigma_1}\right)_T \quad (8)$$

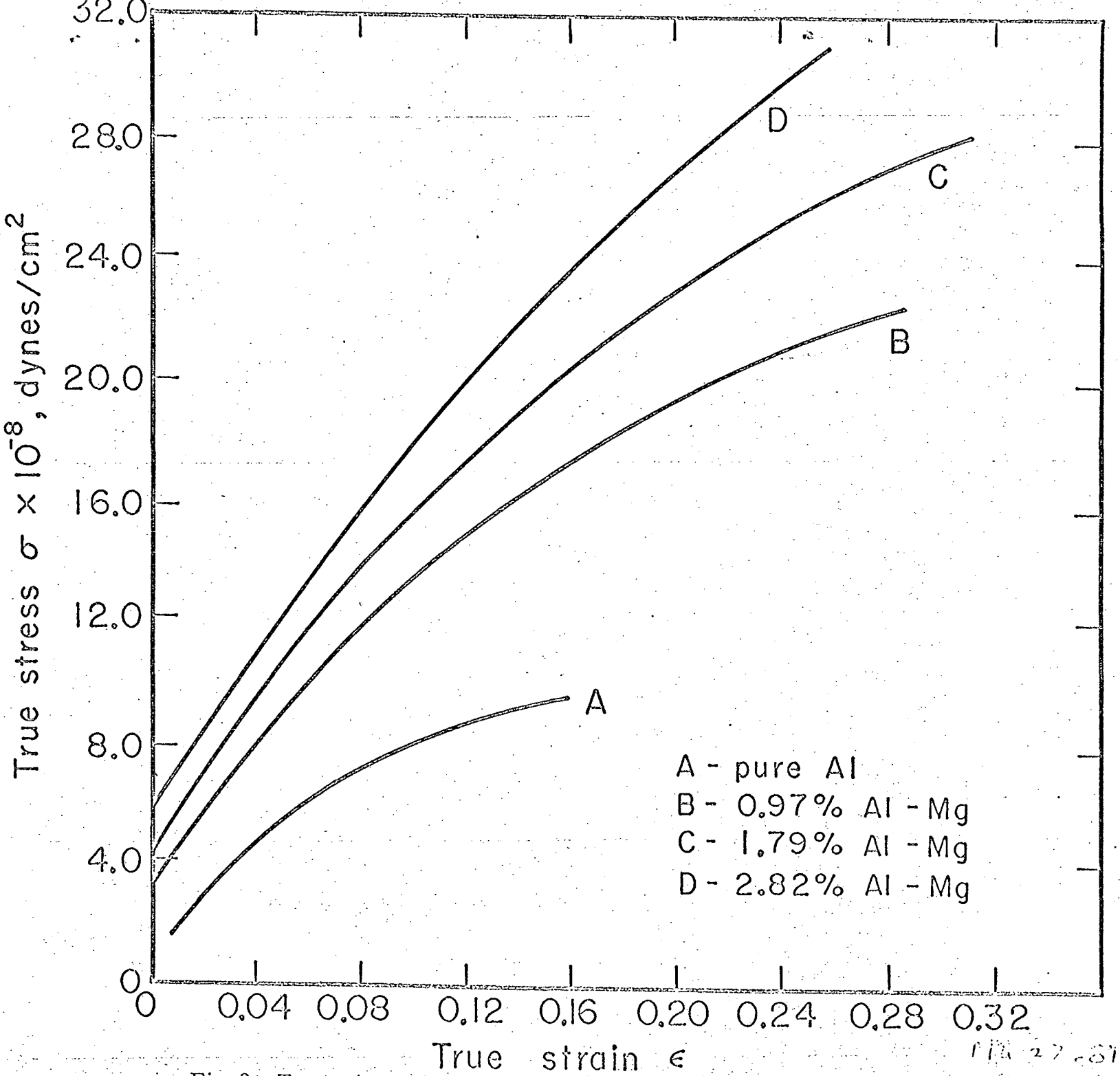

Fig. 2 True-stress true-strain curves for polycrystalline pure Al and Al-Mg solid solutions at 90°K and a strain rate of 1.1×10^{-4} s^{-1}.

UCRL-13183-1

where σ is the true tensile stress, were obtained by means of rapid changes in strain rate from $\dot{\varepsilon}_2 = 1 \times 10^{-4}$/sec. to $\dot{\varepsilon}_1 = 1 \times 10^{-5}$/sec. for tests on all alloys at 90°K, as shown in Figs. 3a and 3b. As shown by Eq. 1, when the strain rate and temperature are held constant, the activation energy, U , is constant provided NA does not change much during a test. The fact that NA is substantially constant was shown proviously.[1] Consequently, F and x as given in Eq. 2 are also constant throughout a test at constant strain rate and temperature. As can be shown by Eqs. 1, 2 and 8,

$$\beta = \left(\frac{\partial \ln \dot{\gamma}^e}{\partial \tau}\right)_T = \frac{x L b}{kT} \qquad (9)$$

Therefore, the decrease in β with stress, as recorded in Fig. 3, reflects how the forest dislocation spacing, L, decreases with true stress. Furthermore, once x is known the value of L can be determined.

In order to establish the values of L and τ^* for the tests conducted at 90°K and the strain rate of $\dot{\varepsilon} = 1 \times 10^{-4}$ per sec, the Cottrell-Stokes ratio was obtained for several strain-hardened states in each alloy. The procedure that was adopted circumvented the difficulties that are introduced as a result of the well-known failure of the mechanical equation of state. The strain-hardened state, represented here by the values of τ^* and L , depends on the temperature and strain rate of the test as well as the total strain. In order to obtain the Cottrell-Stokes ratio for appropriate, well-defined states, each specimen was at first strained to a prefixed true-stress true-strain at 90°K with $\dot{\varepsilon} = 1 \times 10^{-4}$/sec. The load was then quickly removed and temperature change was made. The specimen was then allowed to deform at the new temperature and $\dot{\varepsilon} = 1 \times 10^{-4}$/sec and the yield stress was noted; a series of β measurements was also made in succession. The values of β so obtained were plotted against the stress

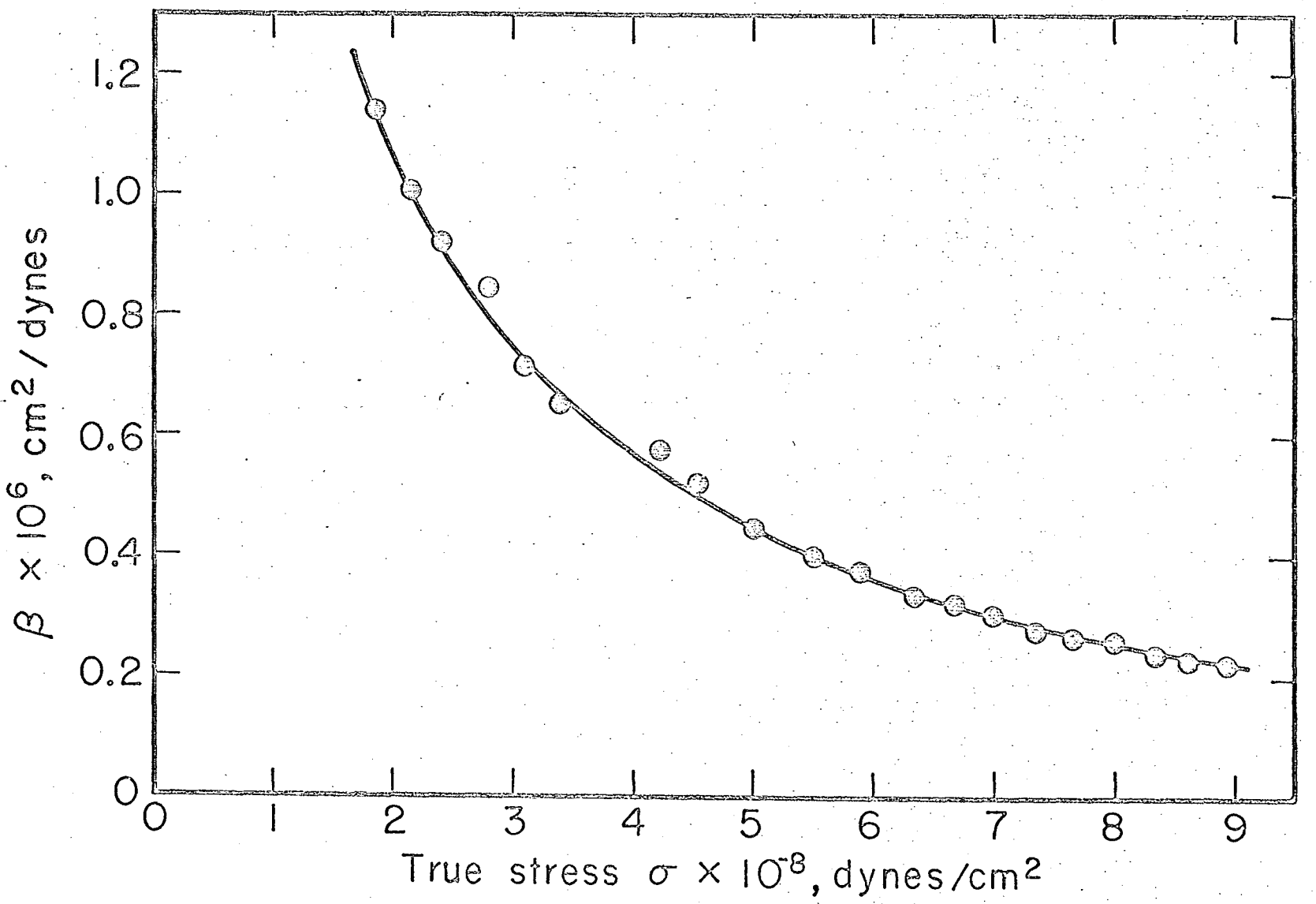

Fig. 3a Variation of $\beta = (\partial \ln \dot{\gamma} / \partial \tau)_T$ with true stress for polycrystalline pure Al at 90°K.

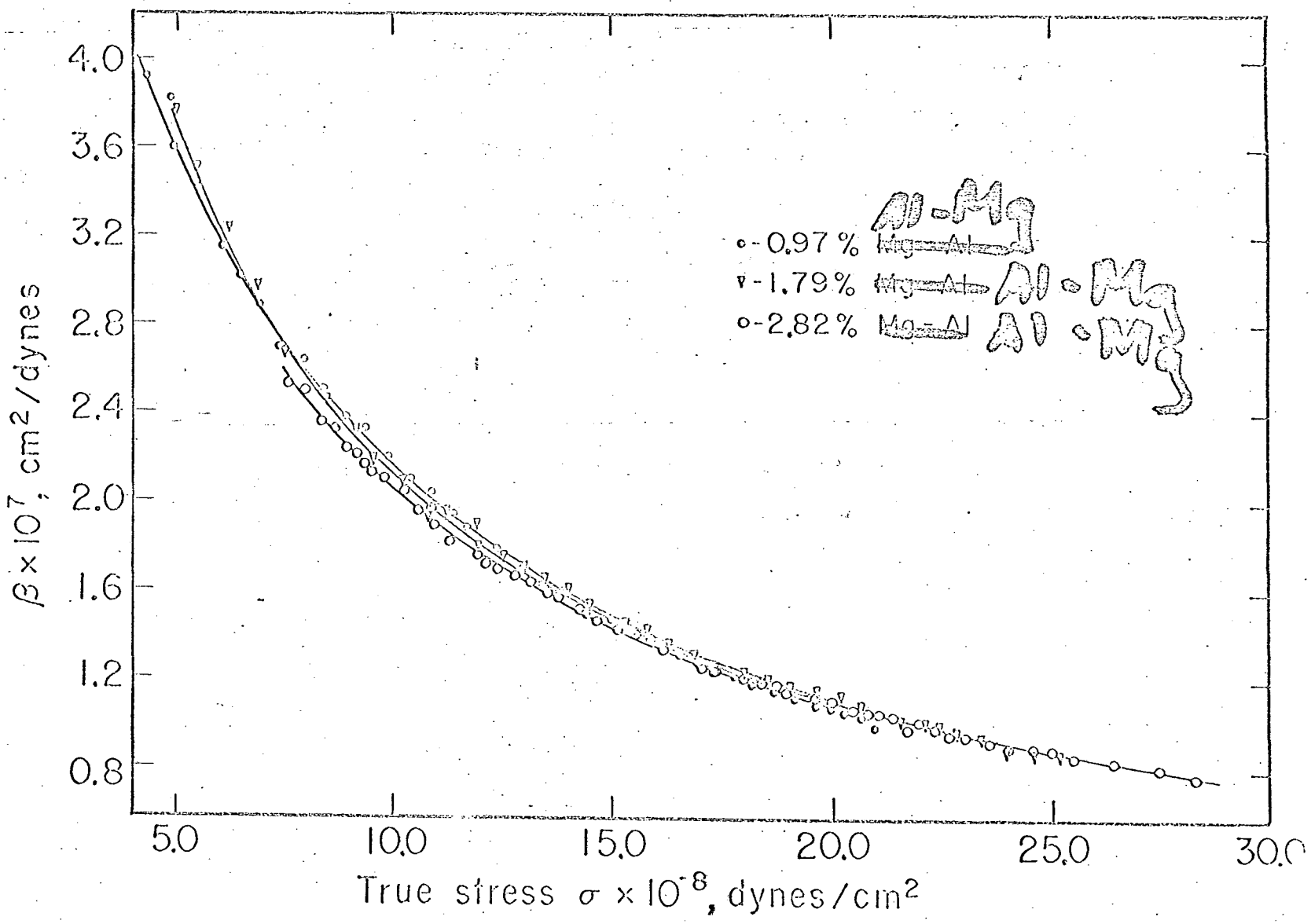

Fig. 3(b). Variation of β with true stress for alloys at 90°K.

MU.27603

and were simply extrapolated to the yield stress at the new temperature. A typical example of the extrapolation of β at different temperatures, for a state corresponding to true-stress true-strain of $7.55 \times 10^8 \text{dyn/cm}^2$ and 0.038, respectively, for 1.79% Al-Mg alloy is shown in Fig. 4. Similar experiments were done for other alloys at different states as is documented in Table II. As shown in Figs. 5a and 5b, the values of $\tau G_o/G \simeq \sigma G_o/2G$ obtained in this way were plotted as a function of $\beta kT = xLb$. Each curve of Fig. 5 refers to a given strain-hardened state as identified by constant value of L and τ^*. Since L is constant, the abscissa, $\beta kT = xLb$, is therefore directly proportional to x.

The value of x was selected to be equal to the Burgers vector b for the tests conducted at 4.2°K. This selection is justified because, U, the energy that must be supplied by a thermal fluctuation in order to effect the completion of a mutual intersection of dislocations is very small at 4.2°K. Consequently, the applied stress must be great enough at this temperature to complete the constriction of the partials. The residual motion required to form the jog is therefore of the order of magnitude of b. Having so selected $x = b$ (at 4.2°K), the values of L were then determined from $L = \beta kT/b^2$ for each strain hardened state at 4.2°K.

From the now known values of L it was possible to plot $\tau LbG_o/G$ vs $x = \beta kT/Lb$, as shown in Fig. 6, for the two specified strain-hardened states of polycrystalline Al that were investigated here. In addition, on the same graph are shown the same data for single crystals of high-purity Al for the initial yield strength (the beginning of easy glide) and for a strain-hardened state that represents almost the maximum limit for the linear range (Stage II) at 160°K, the maximum temperature employed in this study. At slightly higher values of strain hardening, therefore, the

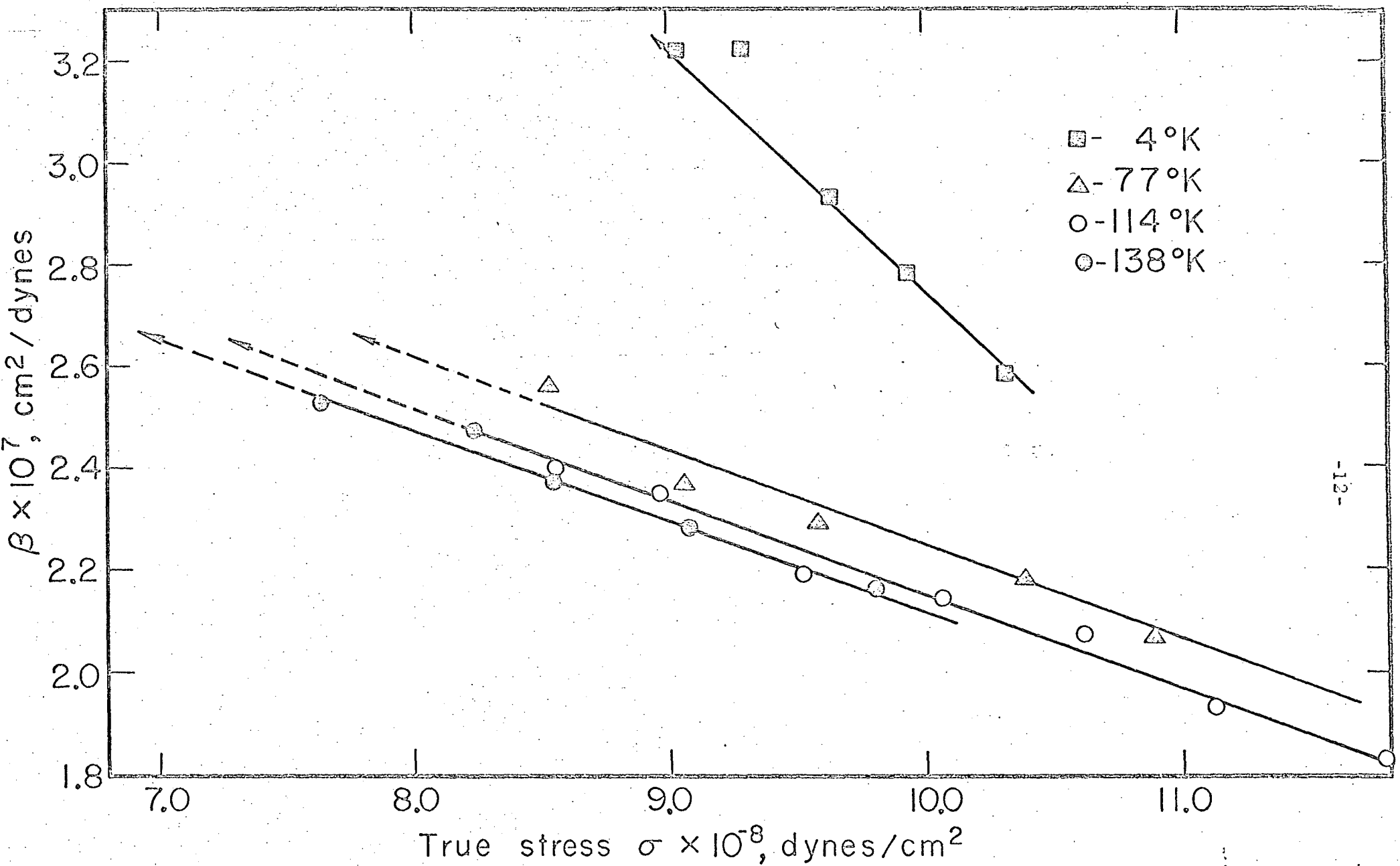

Fig. 4 Extrapolation of β at different temperatures for a given state corresponding to the true-stress true strain of 7.55×10^8 dyn/cm^2 and 0.038, respectively, for 1.79% Al-Mg alloy at 90°K.

Table II. Value of L and $\tau^*_{o_\ell}$ at different states for different materials

Material	STATE: True stress (dyn/cm^2)	True strain	Value of β at 90^oK, $\dot{\epsilon} = 1\times10^{-4}/sec$ (10^{-7} cm^2/dyn)	$\tau^*_{o_\ell}$ (10^8 dyn/cm^2)	Calculated values of L ($10^6 \times cm$)	x (10^{-8} cm)	Density of dislocation $\rho = 3/L^2$, cm^2
Pure Al	2.09×10^9	0.010	10.41	0.86	7.5	5.8	5.3×10^{10}
	2.37×10^9	0.014	9.20	1.01	6.4	5.8	7.3×10^{10}
Alloy (i)	6.64×10^9	0.031	2.91	3.2	2.4	5.3	5.2×10^{11}
Alloy (ii)	5.44×10^9	0.011	3.40	3.35	2.7	5.3	4.1×10^{11}
	7.55×10^9	0.038	2.72	4.95	2.2	5.3	6.2×10^{11}
Alloy (iii)	9.10×10^9	0.028	2.22	5.00	1.8	5.3	9.3×10^{11}
	10.80×10^9	0.042	1.88	5.55	1.6	5.3	11.7×10^{11}

UCRL-10365

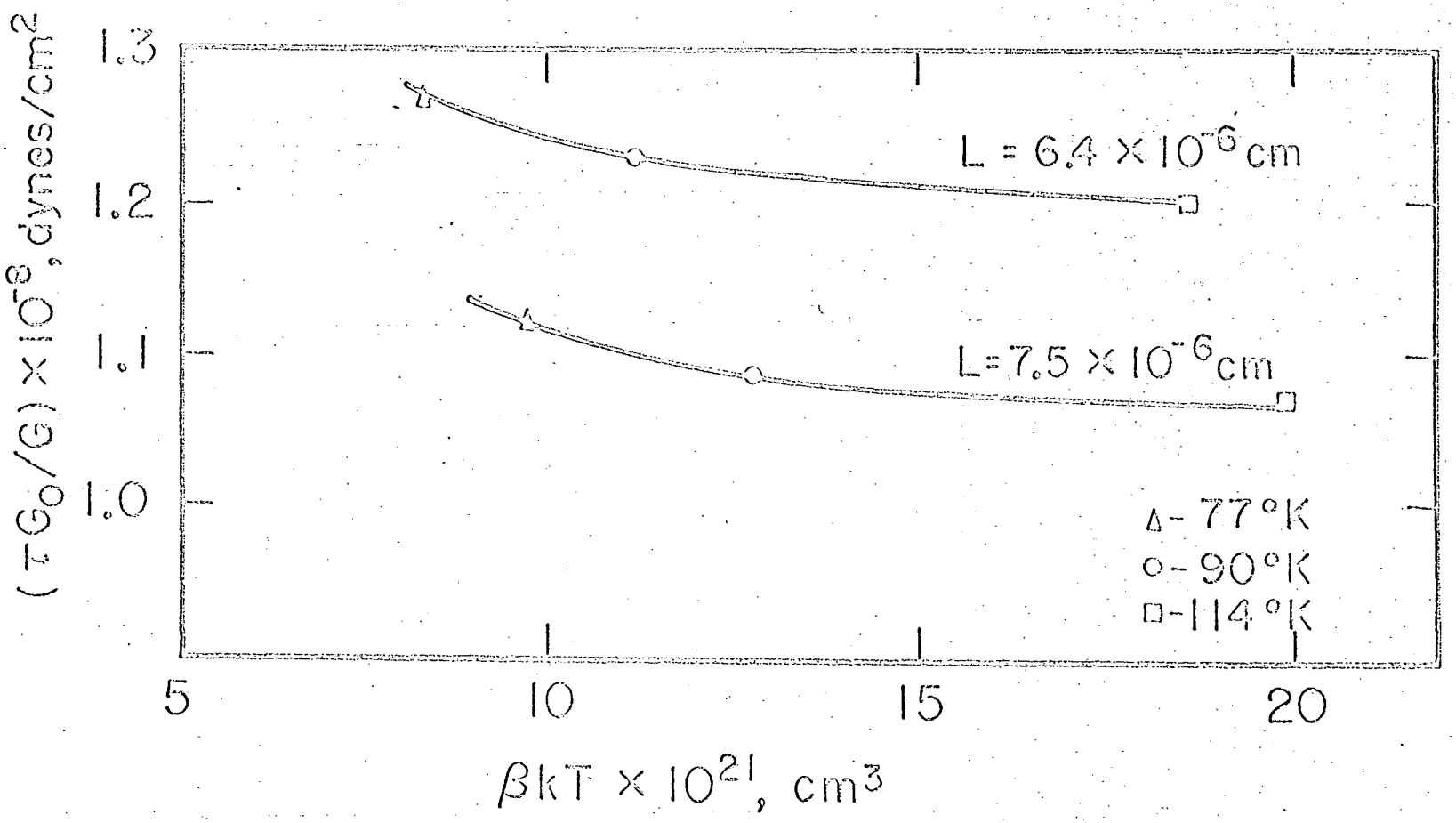

Fig. 5(a). Plot of $\tau G_o/G$ vs βkT for pure Al at two states at $\tau = 1 \times 10^{-4}$ sec.

MU-27605

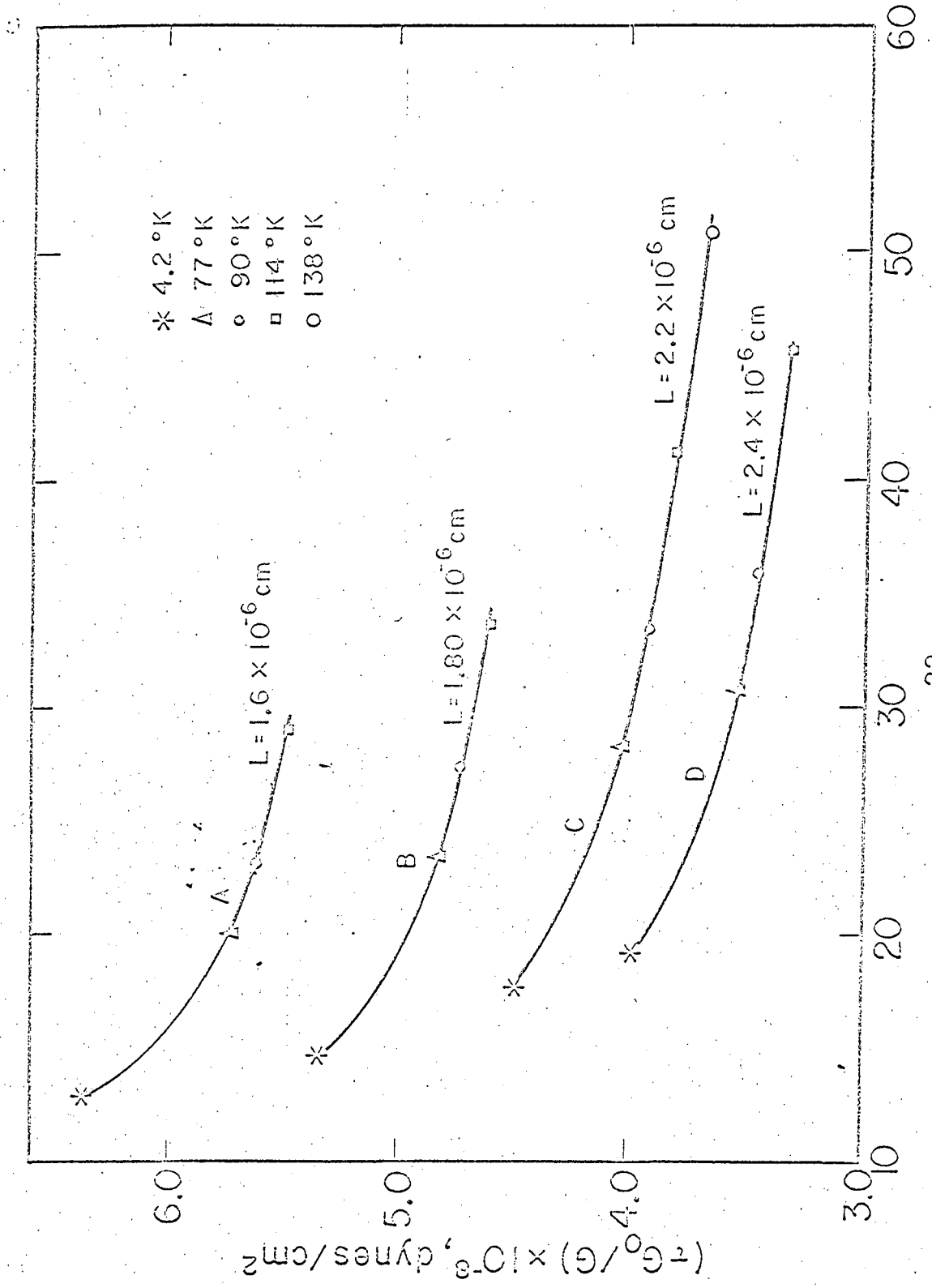

MU-27606

Fig. 5(b). Plot of $\tau G_o/G$ vs βkT for alloys at different states with $\dot{\epsilon} = 1 \times 10^{-4}$ sec: A, B = 2.82%, C = 1.79%; and D = 0.97% Al-Mg.

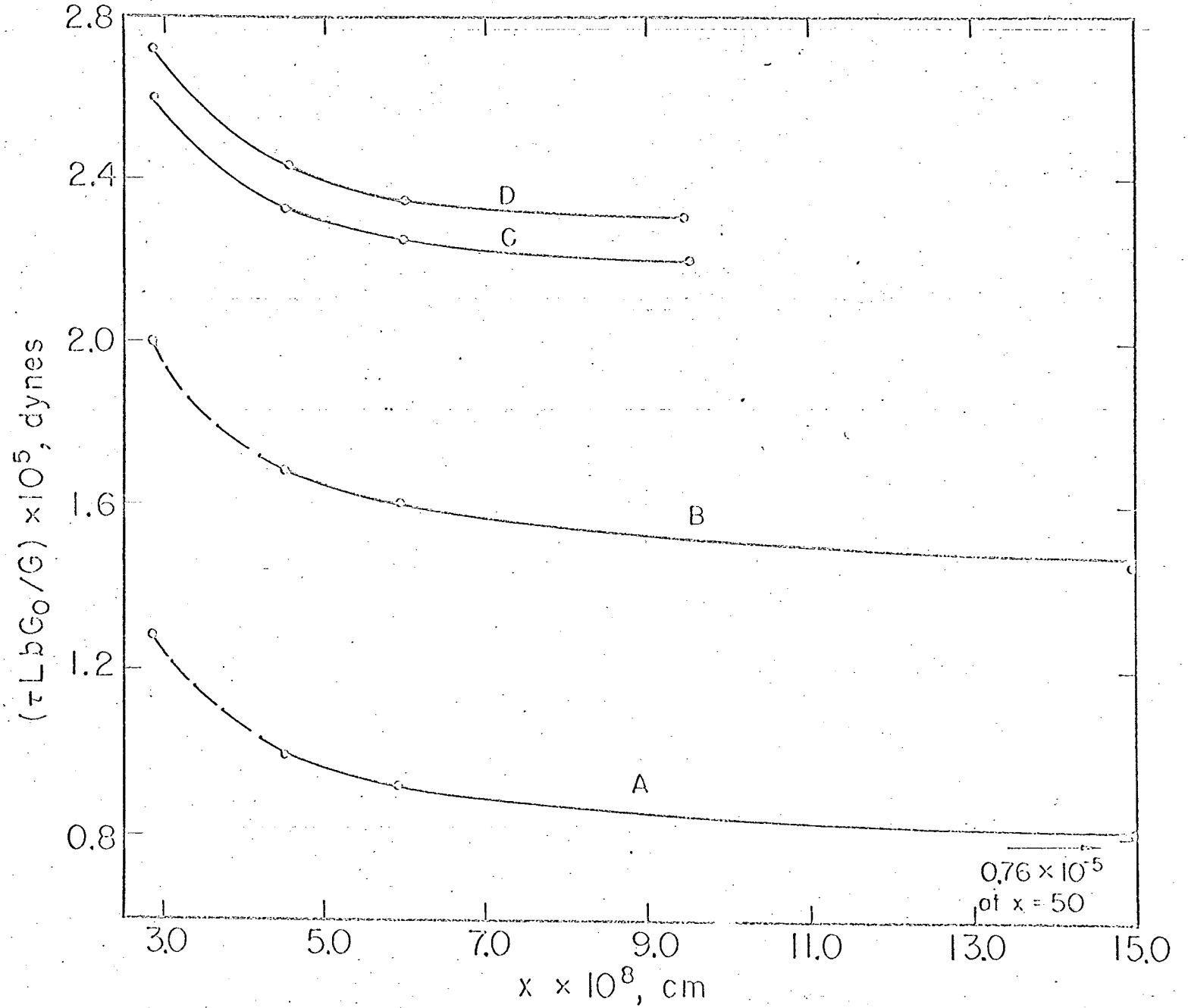

Fig. 6. Plot of $\tau LbG_o/G$ vs x for pure Al single crystals: (A) at a state close to yield point (B) at a state near the end of stage II, and (C, D) for polycrystals at two states with $\dot{\epsilon} = 1 \times 10^{-4}$ sec.

MU-27602

single crystals would enter Stage III of parabolic strain hardening that characterizes the cross-slip mechanism. The various curves of Fig. 6 are identical except for a vertical displacement. This is in agreement with the deductions based on Eqs. 3 and 4, which suggest, for a given metal, that

$$\tau L b G_o/G = F_o + \tau_o^* L b \qquad (10)$$

Therefore, the same F_o - x curve is obtained for polycrystalline Al as applies to single Al crystals, and the differences in the elevation of these curves of Fig. 6 arise from the differences in $\tau_o^* Lb$ for the strain-hardened states that were examined. Since L is now known for these states, the values of τ_o^* can be calculated, assuming, as previously justified[2], that the long-range back stresses, $\tau_{o\ell}^*$, are zero at the beginning of easy glide in the single-crystal data. Therefore, the total back-stress field at the beginning of easy glide is equal to 0.035 Gb/L. From the difference in $\tau LbG_o/G$ represented by the vertical displacements of the curves in Fig. 6, the values of τ_o^* appropriate to each strain-hardened state were calculated, as documented in Table II. Subtracting the values of $\tau_o^* Lb$ from $\tau LbG_o/G$ gives the same F_o - x curve shown in Fig. 1 for polycrystalline Al as was previously deduced from single-crystal data.[2]

A similar analysis was performed on the data on Al-Mg alloys in order to estimate the value of L for the strain-hardened states shown in Fig. 5b. From the values of L for each alloy and state calculated in this way, the data in Fig. 5b were replotted to give $\tau LbG_o/G$ vs $x = \beta kT/Lb$, as shown in Fig. 7. Except for the previously described vertical displacement, these curves are identical (within experimental error) for the

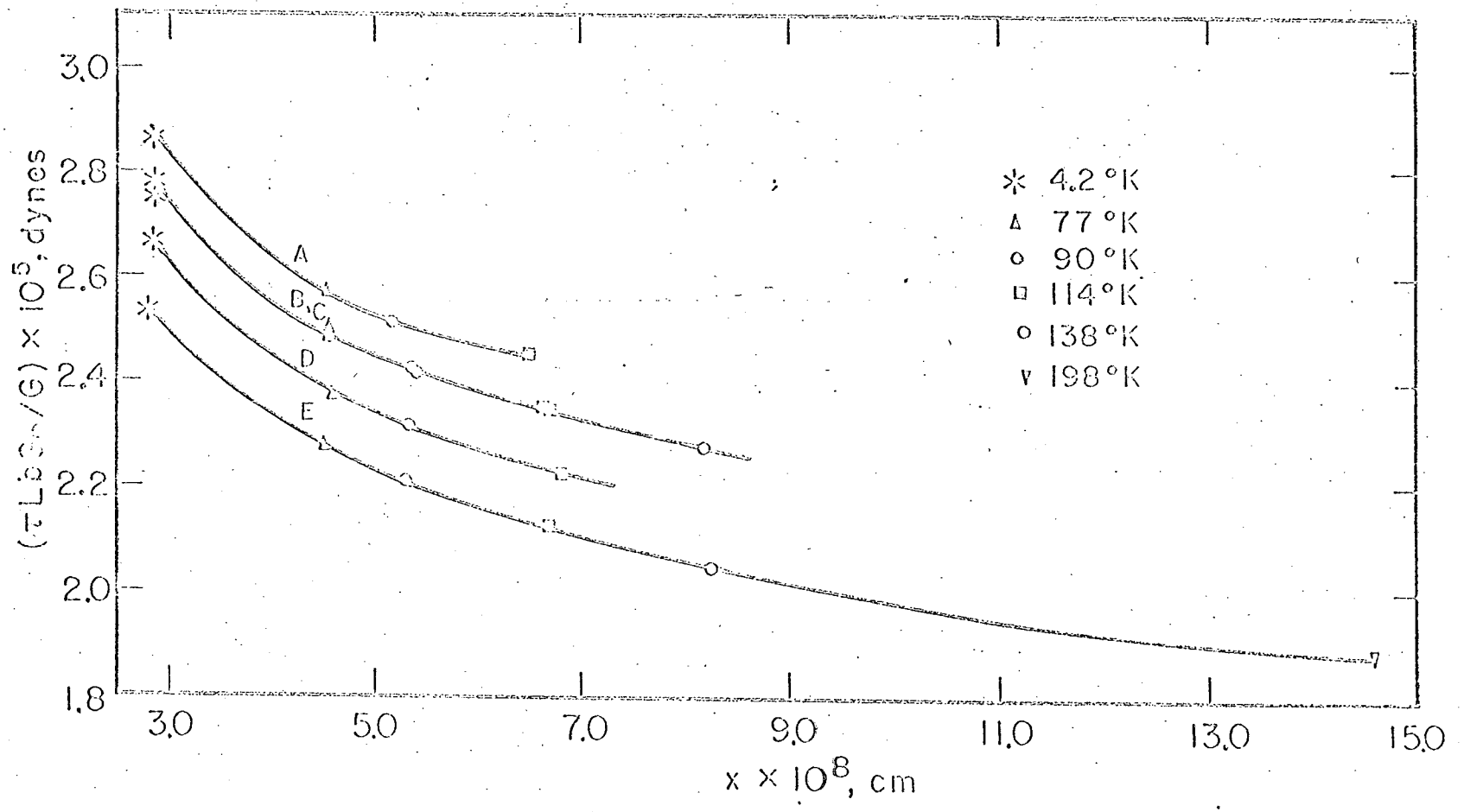

MU-27608

Fig. 7. Plot of τ LbG$_0$/G vs x for alloys at different states with $\dot{\epsilon} = 1 \times 10^{-4}$ sec: A, B = 2.82%; C, E = 1.79%; and D = 0.97% Mg in Al.

various alloys, but they differ from the corresponding curves of high-purity Al in as much as they do not level off as rapidly with increasing values of x. This suggests that greater displacements are required to complete intersection and that the total energy expended in intersection is greater for the alloys. Although the cause of this observation cannot be definitely established exclusively in terms of the observations made here, the results suggest that small initial amounts of Mg might lower the stacking-fault energy of Al.

Whereas the values of τ^*_o for the tested states for polycrystals of pure Al could be established quite accurately from the estimated value at the yield strength of single Al crystals, this procedure could not be used for the Mg alloys of Al, since the single crystal data were unavailable. On the other hand, the value of $\tau LbG_o/G$ in Fig. 7 for the greatest value of x studied is probably only slightly greater than $\tau^*_o Lb$. Therefore, to within this approximation τ^*_o can be calculated for the data of the 1.79% Mg alloys. And correspondingly, the values of $\tau^*_o Lb$ for the remainder of the Mg alloys can be determined from the differences in the vertical displacements of the curves of Fig. 7 and the known values of L for each alloy. The pertinent data are now summarized in Table II.

By use of the data given in Table II and those depicted in Figs. 3a and 3b, it is now possible to deduce the significant strain-hardening trends of the variation of $1/L$ and τ^*_o with strain during tension at 90°K. From a plot of $\tau G_o/G$ against β kT on a log-log sheet shown in Figs. 8a and 8b, values of $1/L$ with strain can be obtained by comparing the values of β kT, using the known value of L for each state. The variation of $1/L$ with strain for each alloy is given in Fig. 9. For a fixed strain rate and temperature of deformation, since F is a constant, we have $\tau G_o/G - \tau^*_{o\ell}$ = constant/Lb. On the basis of the known value of $\tau^*_{o\ell}$ for the states

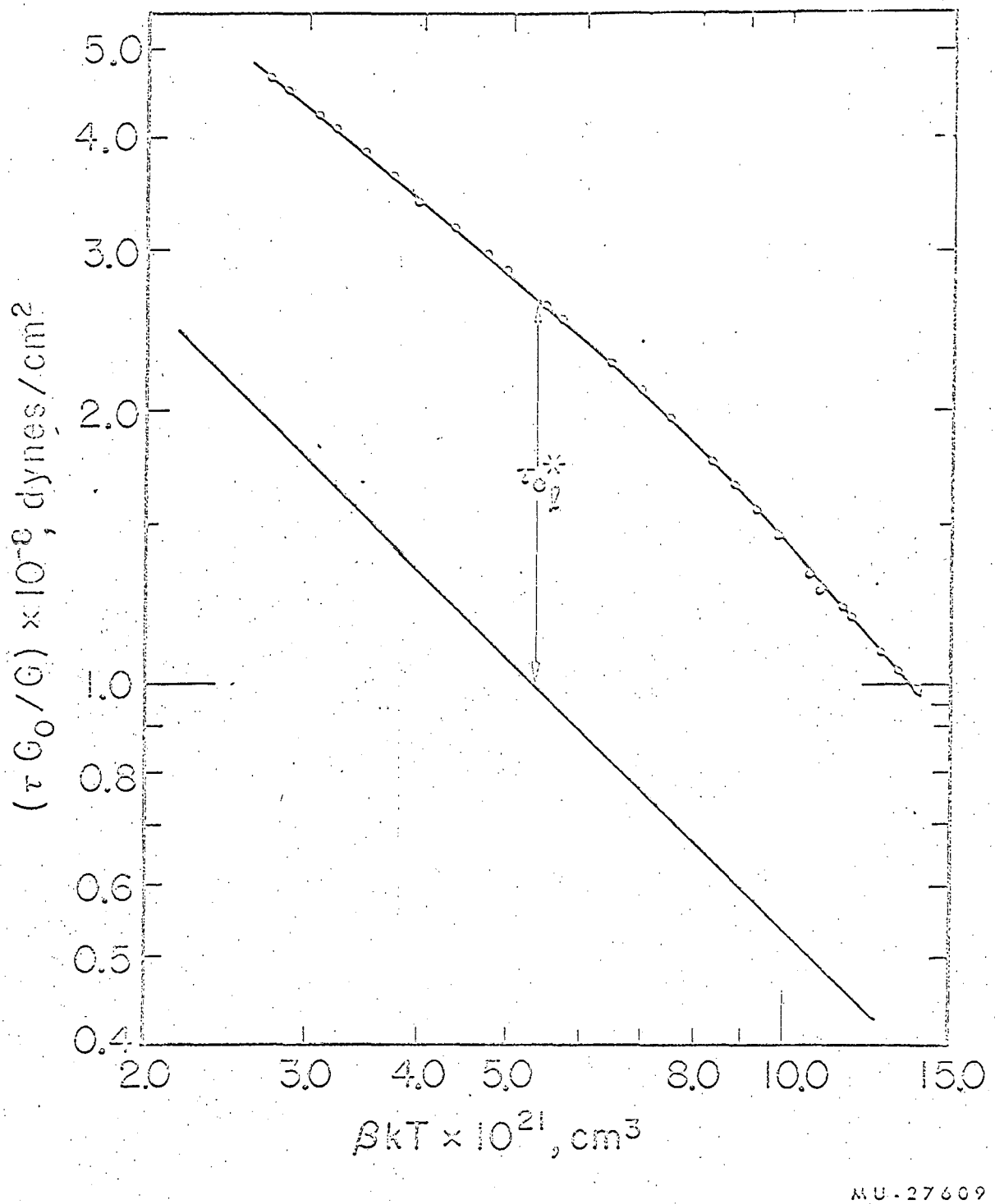

Fig. 8(L). Plot of $\tau G_o/G$ vs βkT for polycrystalline pure Al at 80°K, $\dot{\epsilon} = 1 \times 10^{-4}$ sec.

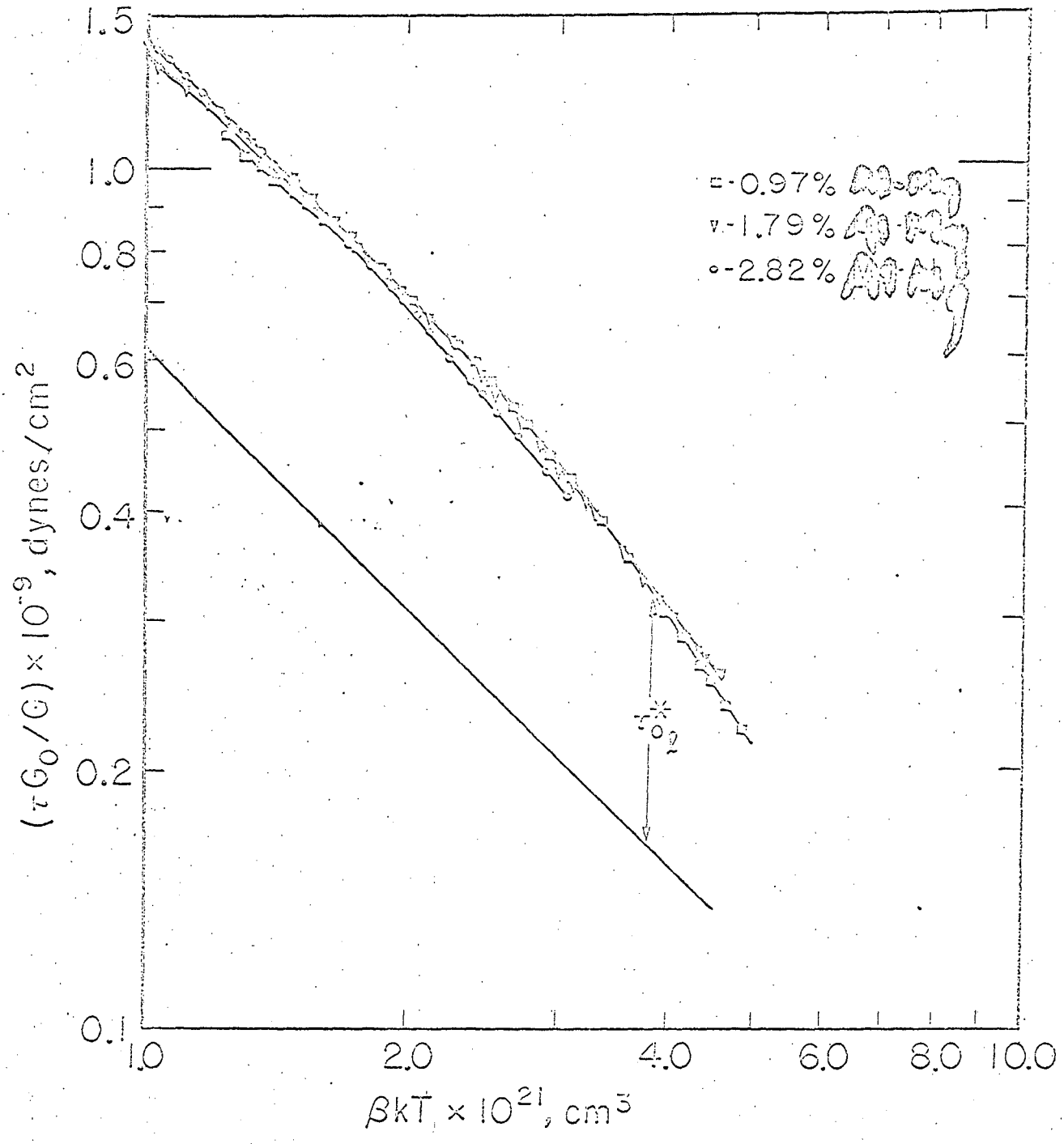

Fig. 8(b). Plot of $\tau G_o/G$ vs βkT for Al-Mg alloys.

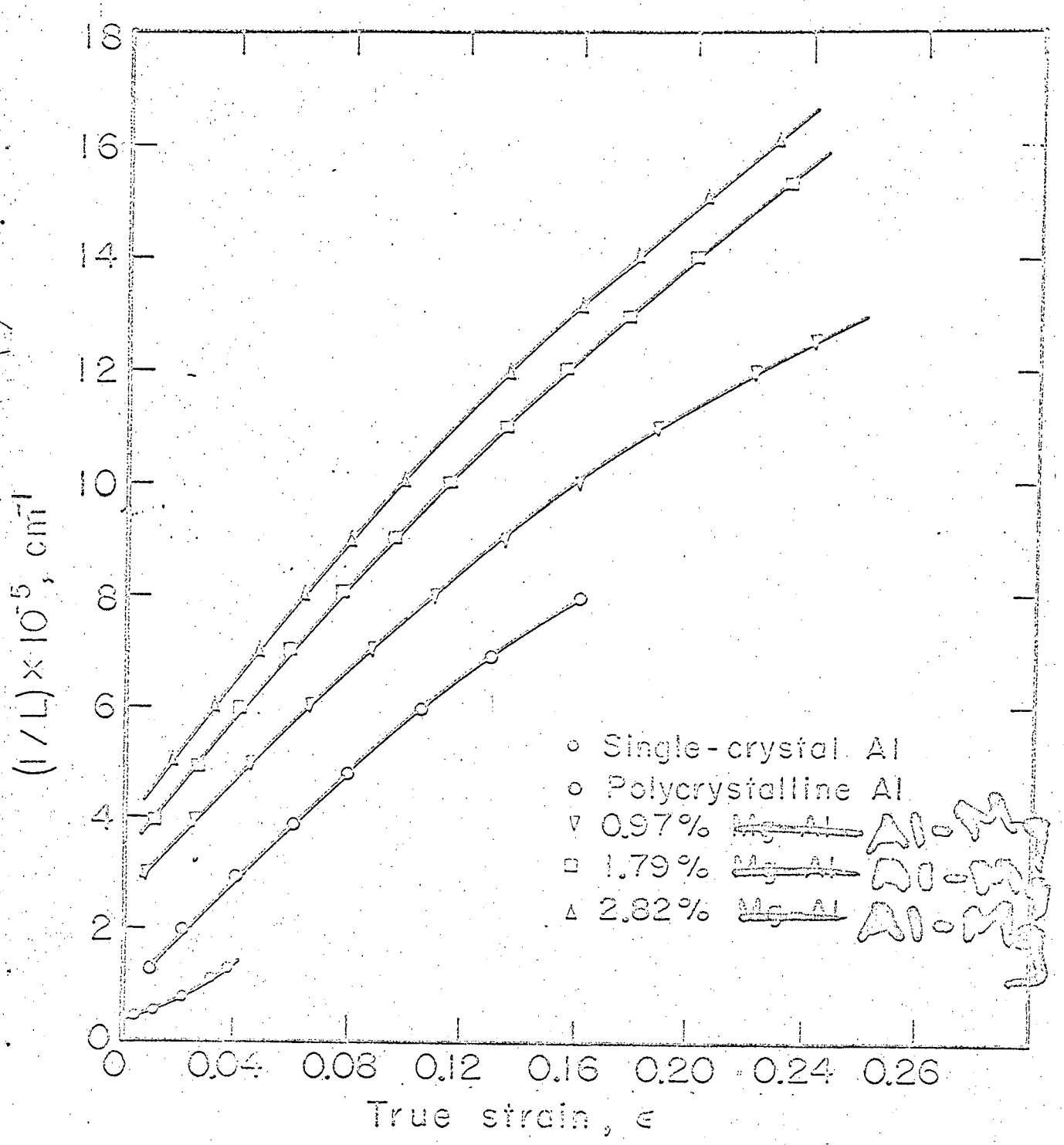

MU-27611

Fig. 9. Plots of 1/L vs true strain for single-crystal and polycrystalline pure Al and for ~~Mg~~ Al-Mg alloys.

shown in Table II, a 45° line is drawn as shown in Figs. 8a and 8b. From the differences of the observed curve and the 45° line, the values of $\tau^*_{o\ell}$ for other strains were obtained, (given in Figs. 10 and 13), as previously justified in reference 2.

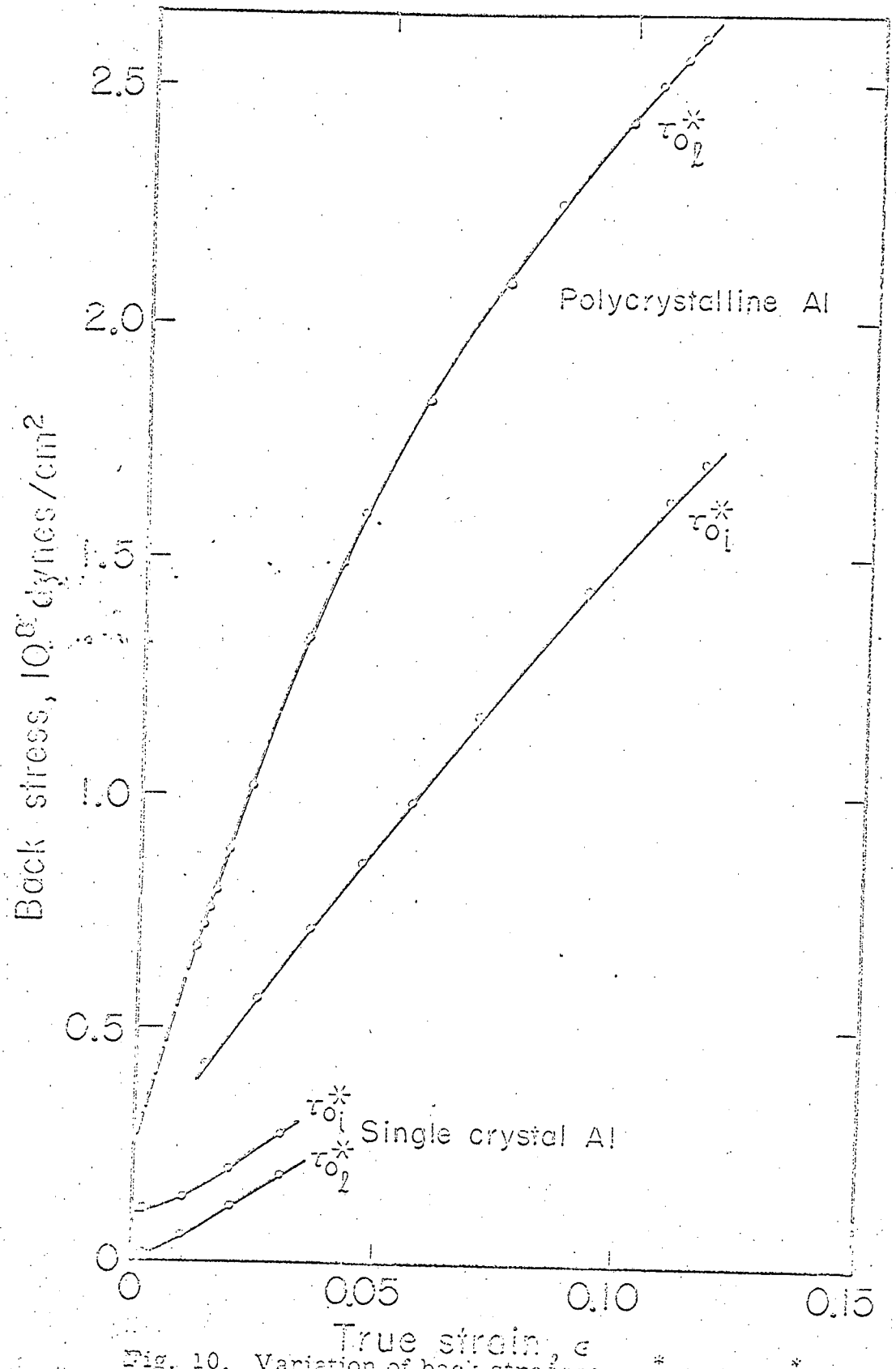

Fig. 10. Variation of back stresses $\tau_{o_\ell}^*$ and $\tau_{o_i}^*$ with strain for single-crystal and polycrystalline pure Al.

MU-27612

III. DISCUSSION

Pure Aluminum

The observed agreement between the F_o - x curve for intersection deduced from polycrystals and that for single crystals has a number of important implications. This curve represents some smeared average value of the force-displacement diagram during intersection of two dislocations. Therefore, the identity of the F_o - x curves for single and polycrystalline aluminum reveals that the smeared average conditions for intersection are substantially the same in the two types of test materials regardless of the pronounced differences in the number of operative slip systems and in the arrangements and densities of dislocations. Furthermore, the upper curve for the single crystals in Fig. 6 represents almost the stress level at which cross-slip takes place since parabolic hardening of Stage III would be initiated at a slightly higher stress level. Since the stress levels for plastic flow in the polycrystals as shown in Fig. 6 are usually much greater than those required to induce cross-slip in single crystals, extensive cross-slip must be taking place in the polycrystalline specimens. In spite of the introduction of this alternative thermally activated mechanism of deformation, the same F_o - x diagram nevertheless remains valid. The obvious explanation is that, over the ranges of conditions investigated here, the two processes are not independent. As cross-slip takes place, the back stresses are relieved and dislocations move up at a rate dictated by the intersection mechanism. Where both processes are mutually dependent, therefore, the analysis for strain rate may be based on either mechanism since either can be considered strain-rate controlling. Consequently, it is reasonable to base the entire analysis here on the intersection mechanism, since cross-slip merely plays the role of relief of the back stress acting on intersecting dislocations.

As shown in Fig. 9, the initial dislocation density ρ, where $\rho = 3/L^2$, is about the same for the single and polycrystalline Al investigated here. The changes in dislocation density with strain are, however, pronouncedly different for the two materials. Over the easy-glide region, $1/L$ for single crystals increases only modestly with strain, and it increases almost linearly with strain over the linear-hardening range of Stage II. Whereas $1/L$ increases slightly less than linearly with strain for polycrystalline Al, its rate of increase with strain is about four times as great as that for single crystals. This difference is due largely to the imposed polyslip that must take place in polycrystalline aggregates.

The major difference between the plastic behavior of single crystals and polycrystalline aggregates is due to the pronounced differences in the back-stress fields as shown by the data recorded in Fig. 10. For pure Al, as shown in Fig. 11, the total back stress τ^*_o arises from the interaction stresses $\tau^*_{o_i} = .035\ Gb/L$ and the long-range-stress fields $\tau^*_{o_\ell}$. Since L is known for each strain, the interaction stresses can be calculated as shown above. Although the interaction and long-range-stress fields are small and about the same order of magnitude for single crystals, they are many times greater for polycrystals; and, for the polycrystals the long-range back stresses $\tau^*_{o_\ell}$ are about twice as great as the interaction stress fields $\tau^*_{o_i}$. These observations are undoubtedly associated with the blockage to slip at the boundaries of dissimilarly oriented grains. Whereas the long-range back stresses in the polycrystalline aggregate at first increase almost linearly with strain, they finally increase less rapidly, as is expected in terms of the effects of relief of the back-stress fields by cross-slip.

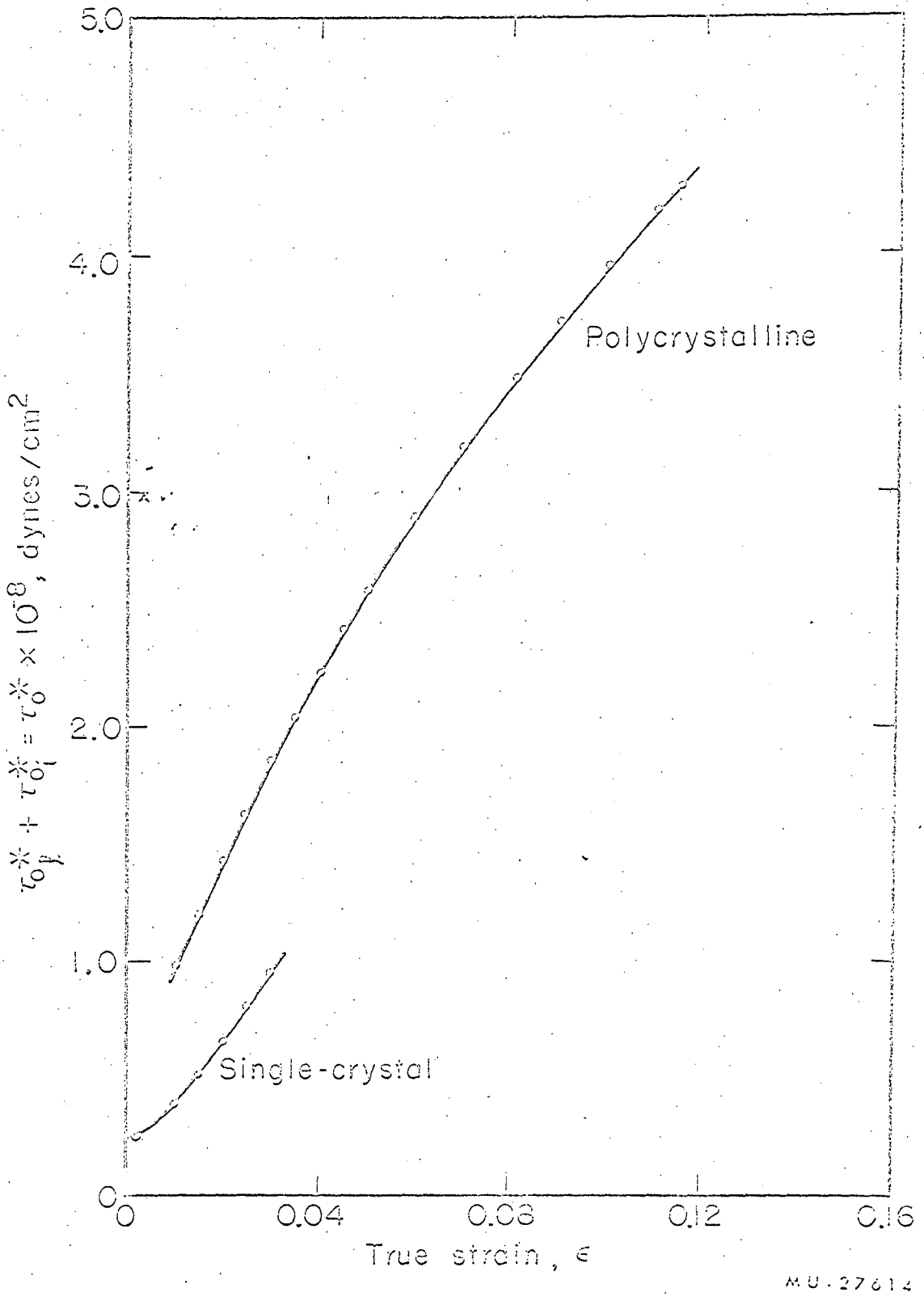

Fig. 11. Variation of τ_0^* for single-crystal and polycrystalline pure Al.

A comparison of the long-range back stresses in single and polycrystalline Al at different values of 1/L is shown in Fig. 12. The ratio $(\tau_o^*)_{poly}/(\tau_o^*)_{single}$ at the same values of 1/L is about 1.6. This coincides well with the factor deduced theoretically by Taylor[9] that $\sigma_{poly} \simeq 2\tau_{poly} \simeq 3.10\,\tau_c$ for the correlation of the flow stress σ_{poly} in polycrystals with the critical resolved shear stress, τ_c, for slip in single crystals. Whereas Taylor wrongly assumed that the comparison might be made at the same shear strains, this analysis reveals that the comparison should be made at the same structure, as given by 1/L. This is in agreement with the suggestion made by Kocks.[10] The higher value of τ_o^* for the polycrystals must then be associated with back stresses of piled-up dislocation patterns that are required to produce appropriate polyslip on five systems in adjacent grains.

The effects of cross-slip also provide a simple explanation for the well-documented failure of the mechanical equation of state, whereas Ludwik[11] and Holloman[12] have suggested that the flow stress is a function of the instantaneous values of the strain, strain rate, and temperature according to $\sigma \equiv \sigma(\epsilon, \dot{\epsilon}, T)$. Several investigators have clearly shown that when these variables are used, the past history of strain, strain rate, and temperature are also involved. A typical result for commercial Al, as obtained previously by Tietz and Dorn,[13] is shown in Fig. 13. When, however, the intersection model is valid, the appropriate relationship is given by $\sigma \equiv \sigma(L, \tau^*, T, \dot{\epsilon})$ as can be seen from Eq. 1. When the tests on single crystals are performed at low temperatures and under conditions such that cross-slip does not occur, L and τ^* are exclusively a function of the strain ϵ and, as shown by Mitra and Dorn,[2] the mechanical equation of state is valid. But when the test is done in the range where cross-slip can occur, τ^* has a lower value than it would have had at that strain if cross-slip had not taken place or if, as occurs at lower test

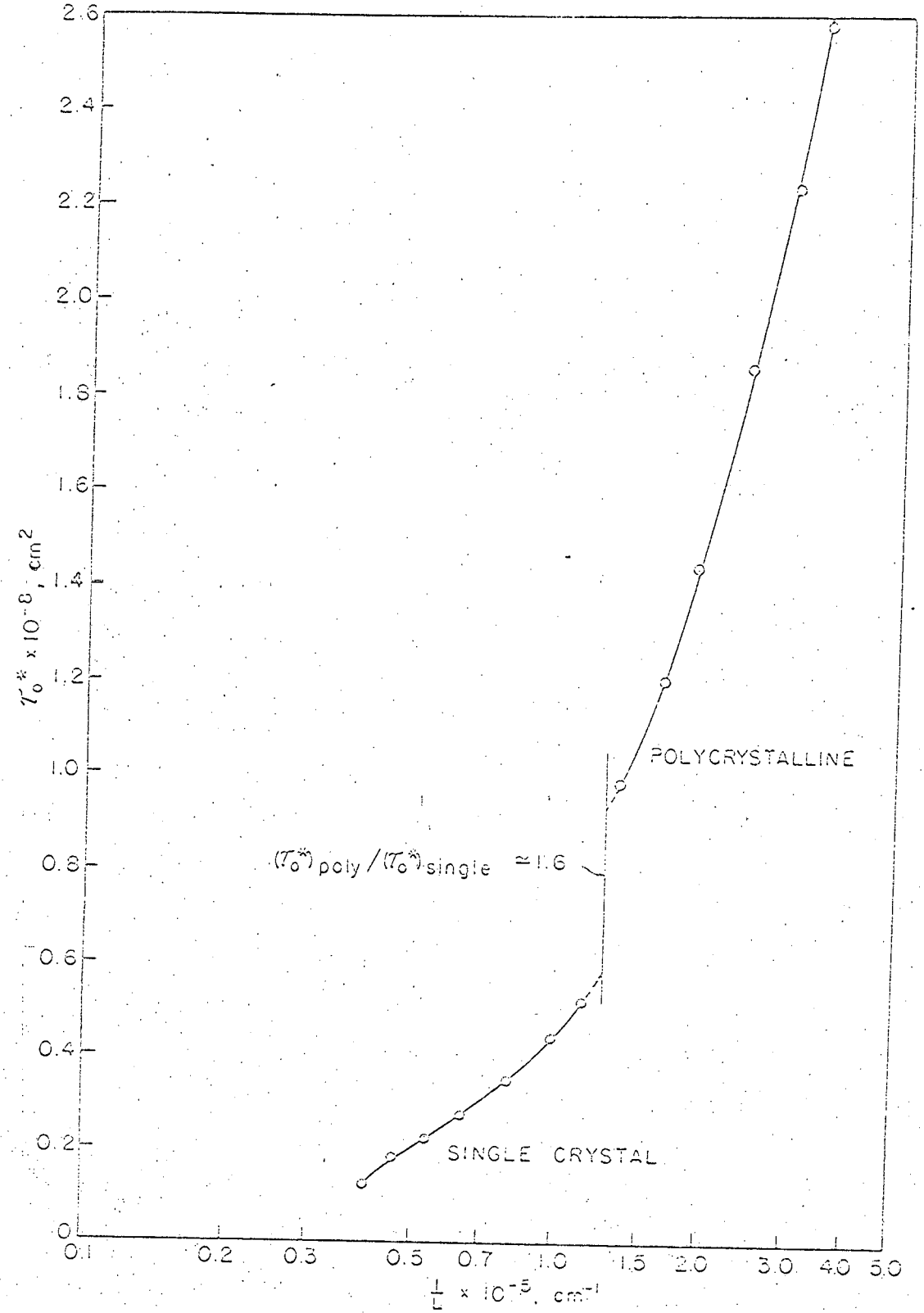

Fig. 12. A comparison of long-range back stresses for the same 1/L in single and polycrystalline pure Al.[30]

temperatures, less cross-slip were obtained. Under these conditions, various combinations of τ^* and L can be obtained as a function of the strain at the different temperatures. For example, first prestraining at a higher temperature and then decreasing the temperature would provide a lower value of τ^* than would have been obtained for the same strain at the lower temperature. And continued straining at the lower temperature would then result in a more rapid increase in τ^* than given at the same stress level for a test done exclusively at the lower temperature. These deductions are in complete qualitative agreement with the data recorded in Fig. 13.

Magnesium Alloys of Aluminum

The strain-hardening characteristics of the polycrystalline Mg alloys of Al differ only quantitatively from those of polycrystalline Al. Previously we have mentioned that the F_o - x curves for all the alloys are similar, but that they differ from that of Al in a way that suggests that the alloys may have a slightly lower stacking-fault energy than pure Al. Thus, a small portion of the increase in the strength of the alloys is due to the slightly higher energies required for intersection. However, a more significant factor in solid solution strengthening arises from the fact that, as shown in Table II, the initial values of 1/L are somewhat greater for the alloys than for pure Al. Undoubtedly, during recrystallization a greater density of dislocations is retained in the alloys as a result of Cottrell atmosphere and Suzuki locking effects. As shown in Fig. 9, the increase in 1/L with strain is greatest for the highest alloy content. For some reason, be it short-range-order strengthening, Cottrell locking, or Suzuki locking, more dislocations are retained in effective positions to require intersection in the

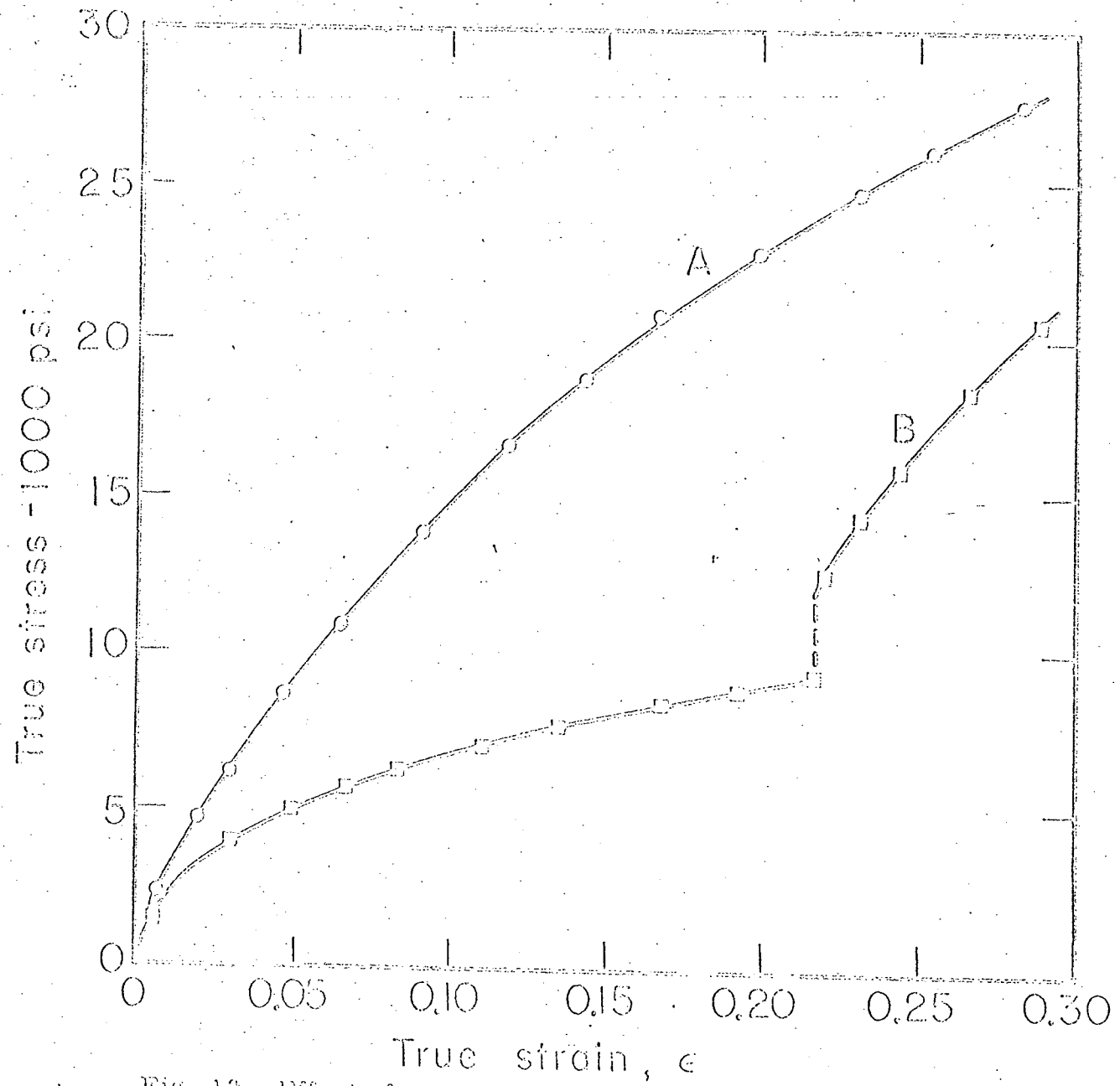

Fig. 13. Effect of prestrain temperature on recovery of pure Al: (A) strain exclusively at 77°K and (B) pre-strained to ϵ = 0.218 at room temperature and subsequently at 77°K. MU-27613

high-Mg-content alloys. And as shown in Fig. 9, the rate of increase in 1/L with strain is also greatest for the highest alloy content. The interaction stresses $\hat{\tau}^*_{o_i}$ for the alloys are shown in Fig. 14. The present data, however, do not permit a separation of the long-range back stresses $\hat{\tau}^*_{o_\ell}$ and the back stresses $\hat{\tau}^*_{o_s}$ due to short-range-order or Suzuki locking. The sums $\hat{\tau}^*_{o_\ell} + \hat{\tau}^*_{o_s}$ are, however, recorded in Fig. 14 and the values extrapolated to zero strain are given in Table III.

Table III. Values of $^*_o + ^*_{o_s}$ at zero strain

Alloy % Mg	$^*_o + ^*_{o_s}$ dyn/cm^2
0	0.25×10^8
0.97	0.60×10^8
1.79	1.00×10^8
2.82	1.50×10^8

These data suggest that only modest increases in the initial flow stress are due to effects of alloying. The major effect of alloying is due to the more rapid increase in $\hat{\tau}^*_o$ with strain for the higher alloy contents.

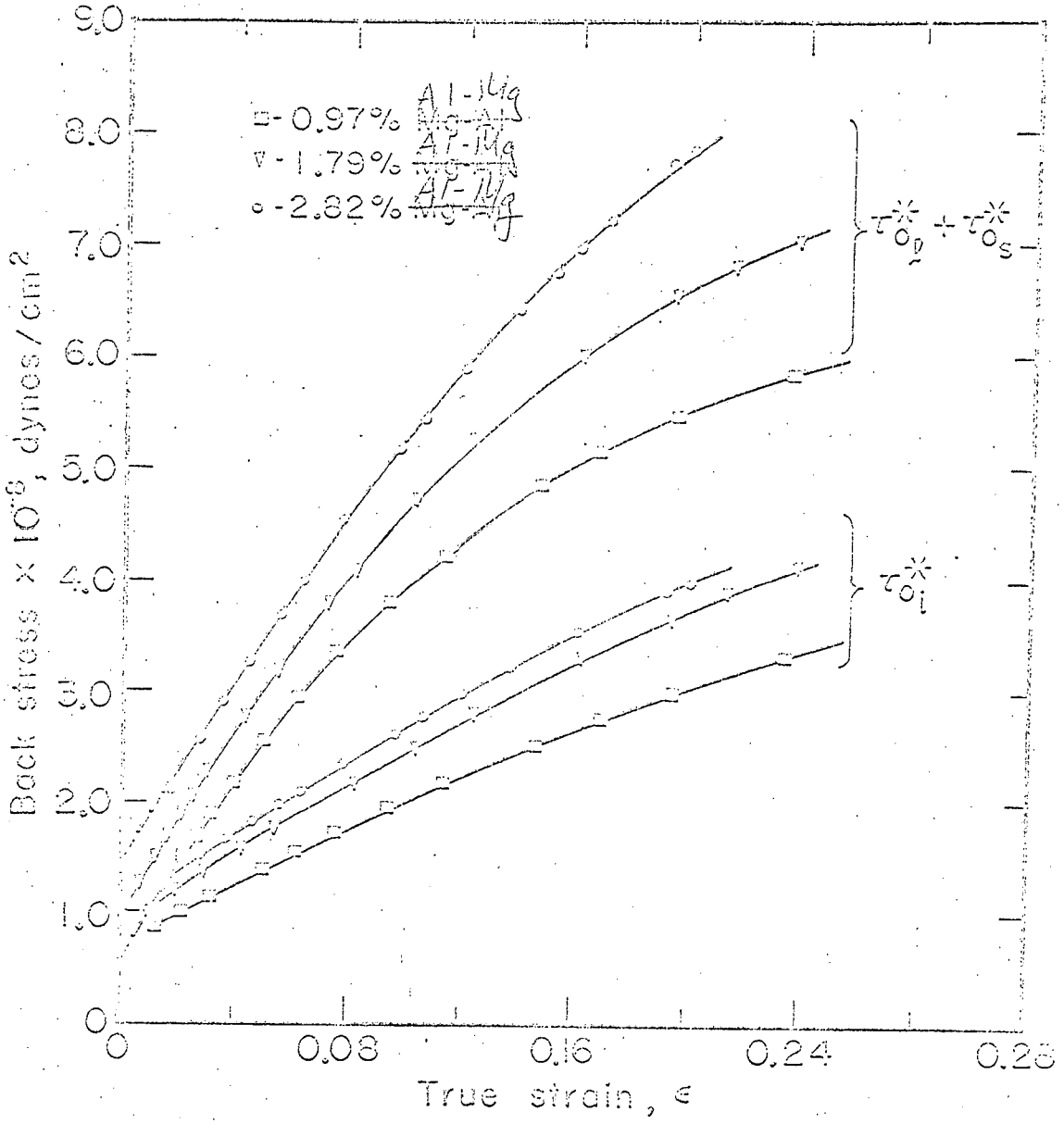

MU-27615

Fig. 16. Variation of $\tau^*_{o_p}$ and $\tau^*_{o_i}$ with strain for Al-Mg alloys at 90°K, $\dot{\epsilon} = 1 \times 10^{-4}$ sec.

IV. CONCLUSIONS

1. The force-displacement diagram for intersection of dislocations deduced from polycrystalline Al data agrees with that deduced from tests on single crystals of Al.

2. The force-displacement diagram for intersection of dislocations in Mg alloys of Al suggest that Mg reduces the stacking-fault energy of Al.

3. The initial mean spacing of the forest dislocations is about the same for annealed polycrystalline Al as for single Al crystals. Annealed polycrystalline alloys of Mg in Al have more dense distribution of dislocations.

4. Polycrystalline Al strain-hardens more rapidly than single crystals because (a) the density of forest dislocations increases more rapidly, (b) the interaction stresses increase more rapidly, and principally, (c) the long-range back stresses show much greater increase with strain.

5. Alloying Al with up to 2.87% Mg results in solid solution strengthening as a result of a small increase in the intersection energy and as a result of solute atom dislocation interactions. A more important effect arises from the increased dislocation density due to alloying. Furthermore, the rate of strain hardening increases greatly with alloying owing to (a) a greater increase in dislocation density, (b) a greater increase in the interaction stresses, and (c) a much greater increase in the long-range back stresses with strain.